Computers and Concrete, Vol. 5, No. 4 (2008) 329-342
DOI: http://dx.doi.org/10.12989/cac.2008.5.4.329

Compaction process in concrete during missile impact: a DEM analysis

Wenjie Shiu*, Frédéric-Victor Donzé and Laurent Daudeville

Laboratoire "Sols Solides Structures et Risques", UMR5521, Université Joseph Fourier, Grenoble Université, BP53, 38041 Grenoble cedex 9, France

(Received November 1, 2007, Accepted April 1, 2008)

Abstract. A local behavior law, which includes elasticity, plasticity and damage, is developed in a three dimensional numerical model for concrete. The model is based on the Discrete Element Method (DEM) and the computational implementation has been carried out in the numerical Code YADE. This model was used to study the response of a concrete slab impacted by a rigid missile, and focuses on the extension of the compacted zone. To do so, the model was first used to simulate compression and hydrostatic tests. Once the local constitutive law parameters of the discrete element model were calibrated, the numerical model simulated the impact of a rigid missile used as a reference case to be compared to an experimental data set. From this reference case, simulations were carried out to show the importance of compaction during an impact and how it expands depending on the different impact conditions. Moreover, the numerical results were compared to empirical predictive formulae for penetration and perforation cases, demonstrating the importance of taking into account the local compaction process in the local interaction law between discrete elements.

Keywords: impact missile; compaction; concrete model; discrete element method.

1. Introduction

When a reinforced concrete structure is impacted, the material is subjected to various states of stress. Near the impactor, the state of stress produces irreversible compaction, whereas farther from this location, the material experiences compression with a moderate triaxial stress state (Burlion, *et al*. 2000). Moreover, in case of a thin concrete target, the compressive wave reflection results in a tensile wave and can produce scabbing (Magnier & Donze 1998). The computational analysis of reinforced concrete walls subjected to this type of loading history must be capable of capturing the key features of the material response under such loads: tensile cracking, compression failure (Donzé, *et al*. 1999), the effect of confinement on the ultimate stress and compaction.

The Discrete Element Method (DEM) (Cundall and Strack 1979), which is an alternative numerical method to continuum-type methods, is used here to study the behavior of concrete structures subjected to rigid impacts. This method does not specify where and how a crack or several cracks occur and propagate, since the medium is naturally discontinuous and is very well adapted to dynamic problems, when a transition from the solid state to a granular flow regime is

* Corresponding author E-mail: wen-jie.shiu@hmg.inpg.fr

observed. However, using solely local elastic-brittle or even elastic-perfectly plastic constitutive laws seem not sufficient to reproduce quantitatively the behavior of the concrete material during the compaction process (Hentz, *et al*. 2004a). In this work, an attempt was made to develop a local elastic-bilinear hardening-damage constitutive law in order to capture the local compaction process which can not be taken into account intrinsically, when using a dense packing of non-deformable discrete elements. The constitutive parameter values were set here using a series of compressive experiment tests on concrete, which were carried out with a high confinement triaxial cell (Gabet, *et al*. 2007). The maximum confining pressure is about 1 GPa which is close to the maximum pressure which can be expected in the impacted area.

After presenting the numerical model in section 1, the local parameter identification process is given in section 2. This model is then applied to simulate the impact of a rigid missile on a reinforced concrete slab. This configuration is based on the experimental CEA-EDF tests (Berriaud, *et al*. 1978). Section 3 deals with the numerical simulations of the impact test. The result for the reference case was compared with the results of a previous DEM model (Shiu, *et al*. 2008a) which used a simple local elastic-brittle model. Then, using the same local parameters in the numerical model, additional simulations were performed to study the evolution of the compacted zone.

2. The DEM model

The discrete element method is used in this work to study the behavior of concrete under strict dynamic loading. The numerical tests were simulated with an open DEM code, YADE (Kozicki and Donzé 2007, YADE 2004). Note that YADE is a code based on the Discrete Element Method, using a force-displacement approach (see Eq. (1a)), Newton's second law of motion, Eq. (1b) and Eq. (1c), describes the motion of each element as the sum of all forces applied on this element. The dynamic behavior of the system is solved numerically by a time algorithm in which the velocities and the accelerations are constant at each time step. The system evolves and an explicit finite difference algorithm is used to reproduce this evolution.

The equations of motion applied to each element are defined by.

$$F_i = K_i U_i \tag{1a}$$

$$F_i = m(\ddot{x}_i - g_i) \quad \text{(Translational motion)} \tag{1b}$$

$$M_i = I\dot{\omega}_i \quad \text{(Rotational motion)} \tag{1c}$$

where F_i is the i^{th} component of the contact force, K_i is the stiffness associated to each element, with K_n in the normal direction and K_s in the tangent direction, U_i is the overlap between two elements in contact, m is the mass of each element, $\ddot{x}_i$ and $\dot{\omega}$ are the translational acceleration and rotational acceleration respectively, g_i is the gravitational acceleration, M_i is the resultant moment acting on each element and I is the moment of inertia. During the calculation cycle, the force-displacement law (Eq. (1a)) is calculated first, then the new element's position will be updated by the law of motion (Eq. (1b), Eq. (1c)).

To reproduce correctly the behavior of the cohesive material, the moment is also transferred between two interacting elements (Belheine, *et al*. 2008, Iwashita and Oda 2000). The relative rotation angle, θ_r, was calculated, and has been put together with the rotational stiffness, k_r, the elastic moment between two elements in contact can be expressed by:

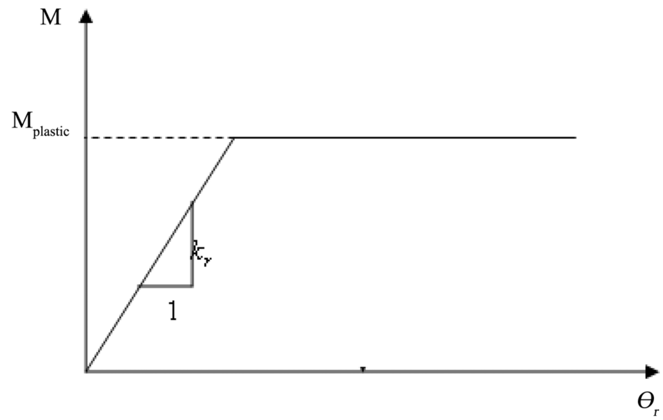

Fig. 1 Evolution of the moment transfer law

$$M_{elastic} = \sum \theta_r * k_r \tag{2}$$

If the actual moment is superior to the threshold of the elastic limit, then the plastic moment will take place. The plastic moment is defined by:

$$M_{plastic} = \eta * F_n * R_{avg} \tag{3}$$

where η is the control factor of the elastic moment limit, F_n is the normal contact force and R_{avg} is the average radius of two interacting elements. Thus, an elastic-plastic behavior is involved in this law (see Fig. 1);

Energy dissipation was also taken into account in the numerical model. The energy involved between two interacting elements is dissipated through frictional sliding for which the Coulomb internal friction angle and the cohesion C, are defined. Thus, the sliding criterion can be written as:

$$F_{s,\max} = F_n \tan\phi_i + C * S_{int} \tag{4}$$

where $F_{s,\max}$ is the maximum tangent force, F_n is the normal contact force and S_{int} is the average cross section of the two interacting elements. If the shear contact force exceeds $F_{s,\max}$, then the sliding mode is activated.

Moreover, a local non-viscous damping is used (Cundall and Stracks 1979), where the damping force is put together with the equation of motion such that,

$$F_{(i)} + F_{(i)}^d = M_{(i)} A_{(i)} \tag{5}$$

where $F_{(i)}$, $M_{(i)}$, and $A_{(i)}$ are the generalized force, mass and acceleration components respectively, and $F_{(i)}^d$ is the damping force

$$F_{(i)}^d = -\alpha \left| F_{(i)} \right| \mathrm{sign}(V_{(i)});$$
$$\mathrm{sign}(y) = \begin{cases} +1, & \text{if} \quad y > 0 \\ -1, & \text{if} \quad y < 0 \\ 0, & \text{if} \quad y = 0 \end{cases} \tag{6}$$

where α is the numerical damping.

2.1. The updated local constitutive law of the numerical model

Concrete can be considered as an isotropic elastic quasi-brittle material. The definition of the limit bearing capacity of concrete depends strongly on the loading situations. The proposed local constitutive law has been developed according to the experimental results obtained from high confinement triaxial tests (Gabet, *et al*. 2007).

Fig. 2 shows the updated local constitutive law of concrete, which only concerns the normal interaction force between two discrete elements. This normal force can be split into two parts, the compressive and the tensile components. During compression, concrete first undergoes an elastic response (section AB), which is calculated by Eq. (7):

$$F_n = K_n * (D_{ij} - D_{init}) \tag{7}$$

where F_n is the normal contact force, K_n is the tangent stiffness, D_{ij} is the actual distance between element i and element j and D_{init} is the initial equilibrium distance. Note that $K = E * R_{avg}$, where E is a reference Young's Modulus and R_{avg} is the average radius of two interacting elements. Doing so, the tangent stiffness K_n depends on the size of the elements.

If the interaction distance exceeds the elastic limit distance (D_1), then the hardening plastic behavior takes place (Section BC and CD on Fig. 2), which is characterized by two successive stages. These two stages involve two different stiffness coefficient controlled by two ratios ζ_1 and ζ_2, representing the observed response of the concrete material at extreme loading conditions (Gabet, *et al*. 2007). Note that, in section BC, the unloading path follows an irreversible behavior controlled by a softer coefficient K_{n_unload}.

The tensile part (section AE on Fig. 2) uses the same tangent module (K_n) as the compressive section AB. After the tensile force has reached its maximum value, $F_{t\,\max}$, which is calculated by

$$F_{t\,\max} = F_{c1} * \gamma_t \tag{8}$$

where F_{c1} is the maximum elastic compressive force and γ_t is an amplified factor to control the value of $F_{t\,\max}$, a softening behavior will occur with a modified tangent stiffness $\dfrac{K_n}{\zeta}$, where ζ is the softening coefficient (See Fig. 2).

If the interaction distance exceeds the rupture distance, $D_{rupture}$, then the interaction force is equal to zero: the cohesive link breaks.

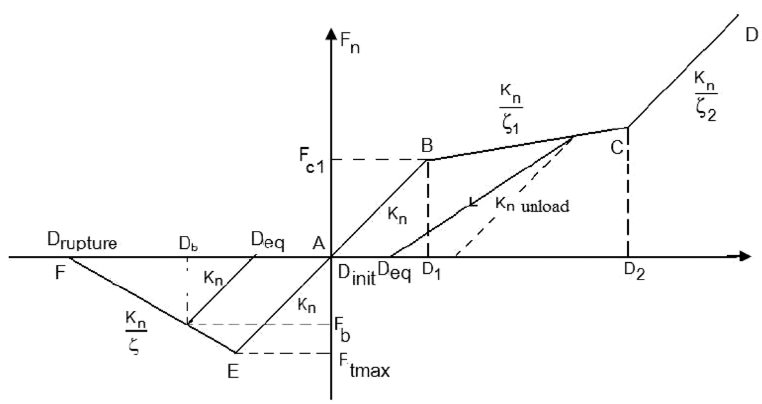

Fig. 2 Local normal interaction force for discrete elements representing concrete

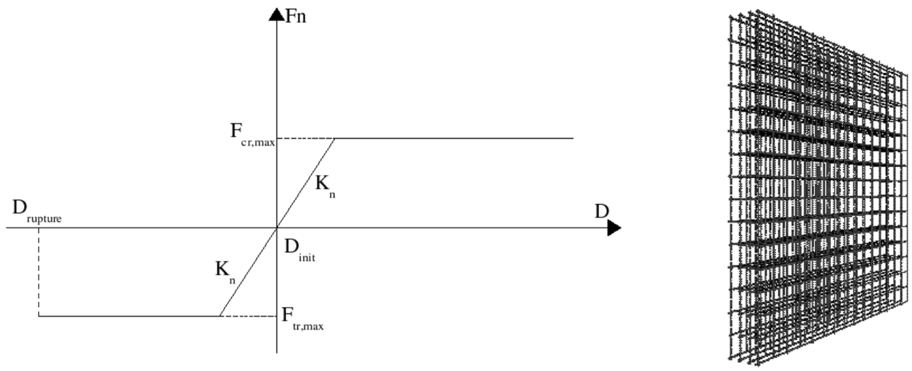

Fig. 3 Local constitutive law of the reinforcement and the spatial arrangement of the reinforcement

2.2. Introducing reinforcement

A full reinforced concrete target has been simulated for the missile impact test. The steel rebar elements have been evenly placed to form a regular grid (see Fig. 3). The numerical rebars have the same diameter as the real rebars. The local interaction between the rebar's discrete elements is shown in Fig. 3. An elastic-plastic constitutive law has been used to represent the behavior of steel. The loading behavior is the same in tension and in compression, i.e., the maximum elastic compressive force, $F_{cr,\max}$, is equal to the maximum elastic tensile force, $F_{tr,\max}$. Furthermore, a tensile breaking strength is introduced: when the distance between two rebar elements exceeds $D_{rupture}$, then the rebar breaks.

2.3. The model calibration process

Using the DEM approach, the impacted wall is represented by a set of discrete elements. Local constitutive parameters are assigned to each of the interaction force between the elements, such that the macroscopic behavior of the entire set is representative of the real material at the scale of the structure. To assign the values of the local constitutive parameters, a calibration procedure, similar to previous work (Hentz, *et al*. 2004b, Belheine, *et al*. 2007) is used. It is based on the simulation of quasi-static uniaxial compression/traction tests. Here, a compression test model is developed in YADE for a standard-sized specimen, with the following characteristics:

• a compact, polydisperse discrete element set is generated,

• an elastic compression test is run with local elastic parameters given by the "macromicro" relations (Hentz, *et al*. 2004b),

• compressive rupture axial tests are simulated to deduce the plastic local parameters.

Fig. 4 shows the results of the simple compression test. The numerical simulations fit well to the experimental ones. By performing these tests, the local parameters (ζ, C, θ_i, ...) have been calibrated. However, performing this simple uniaxial compression test is not sufficient to obtain the full plastic response shown previously in Fig. 2. It is thus necessary to calibrate the plasticity stiffness ratios ζ_1 and ζ_2, with a hydro-static test at a high confining pressure. The 650 MPa test was used as comparison. The result is shown in Fig. 4. Using the same elastic parameter as in the uniaxial compression test, the numerical result agrees well with the experimental test. It has also

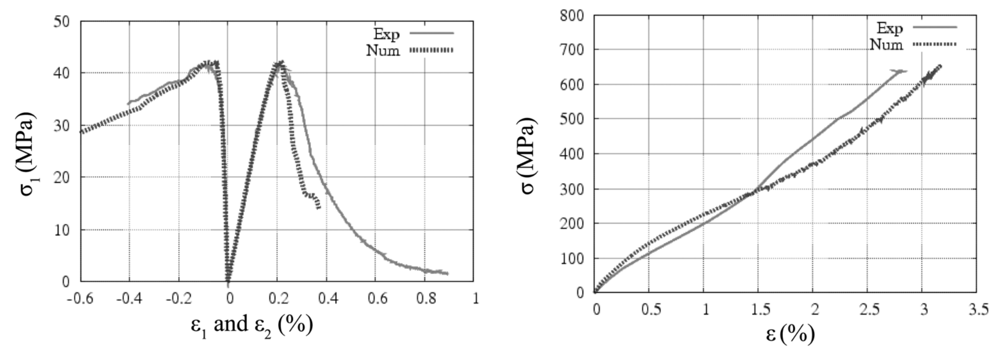

Fig. 4 Strain-stress curves of the uniaxial compression test (left) and the hydro-static test with a confinement of 650 MPa (right)

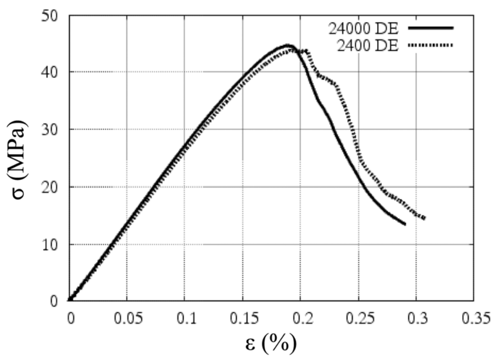

Fig. 5 Strain-stress curves of the uniaxial compression test for two samples of identical size but with different discretization. The plain line and the dotted lines represent respectively, the sample made of 24 000 discrete elements and 2400 discrete elements

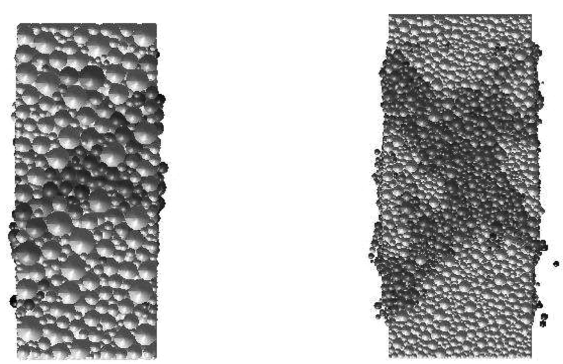

Fig. 6 On the left, 2400 DE, on the right 24000 DE for two samples of identical size. The darker the color of a DE is, the more cohesive links it has lost, this value indicates the amount of local damage

been verified that the discretization, i.e., the size of the discrete elements, has little influence on the response of the medium. This property is particularly important in the present case, since the model is used at a macro-scale and it is of great concern that the results do not depend on the model resolution, which is often imposed by the computation capabilities. The stress-strain curves resulting from the compressive uniaxial tests are presented in Fig. 5, where it is verified that the differences

Table 1 Values of the local parameters

Parameters	E (GPa)	C (MPa)	θ_i (degree)	ξ	γ_t	ξ_1	ξ_2
Value used	30	4	30	5	0.1	10	0.4

due to the discretization remain small in the distribution size range used in the model. The state of the damage is shown in Fig. 6, where the discrete elements have been colored as a function of the ratio between the number of broken links and the number of initial cohesive links. As the damage increases, the color darkens.

The local constitutive parameters have now been fully calibrated. The parameters chosen for simulations are reported in Table 1.

3. Modeling impact tests

3.1. Experimental test

The impact experiments were performed by the French Atomic Energy Agency (CEA) and the French Electrical power Company (EDF) on reinforced concrete slabs (Berriaud, *et al*. 1978). The objective of this work is to show how the local compaction appears and extends during dynamic loading. An impact reference case has been chosen for which the target size was 1.46 m × 1.46 m × 0.208 m. In this case, a flat nose missile was used, and its weight was 34.5 kg and its diameter was 0.278 m, with an impact velocity of 151 m/s.

3.2. Numerical impact configuration

The total number of Discrete Elements used in the concrete slab was about 20 000, with a radius distribution size ranging from 0.005 m to 0.02 m. This resolution size was chosen based on the rebar's diameter, which imposed the minimum discrete element size. The total number of the rebar elements was 17408 and all of them had a radius of 0.005 m. The local parameters of the impact tests are kept the same as those of the static calibration tests. The numerical damping factor is set to 0.1.

The missile was simulated by a set of discrete elements which have the properties of steel. The missile was initially placed just beside the surface of the target with a given initial velocity. The impact configuration (position and orientation) has been set as close as possible to the observed experimental configuration, as shown in Fig. 7. Since in the real test case, the slab is maintained on four sides: these boundary conditions have been reproduced by fixing a 10 cm layer of discrete elements on these four sides of the slab.

3.3. Numerical results for the reference case

The numerical results of the reference case (case presented in the section 3.1) are shown in Fig. 8. At this impact velocity (151 m/s), the slab was just perforated.

The numerical simulation was compared not only to the experimental data obtained by the CEA and EDF, but also to a previous numerical simulation (Shiu, *at al.* 2008a) which had been run with a commercial discrete element code (PFC^{3D}, 2003) in which only a local elastic-brittle law was

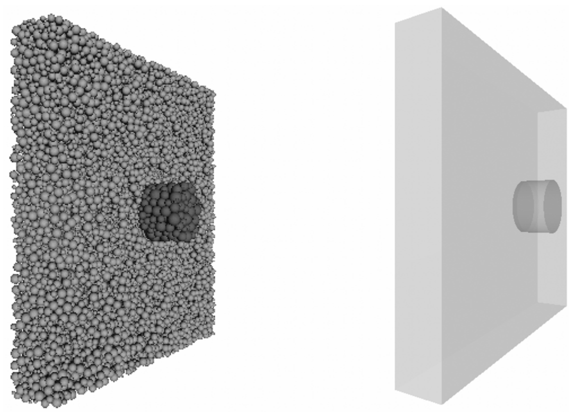

Fig. 7 On the left, the initial discrete elements configuration is represented and on the right, the outlines of this numerical model

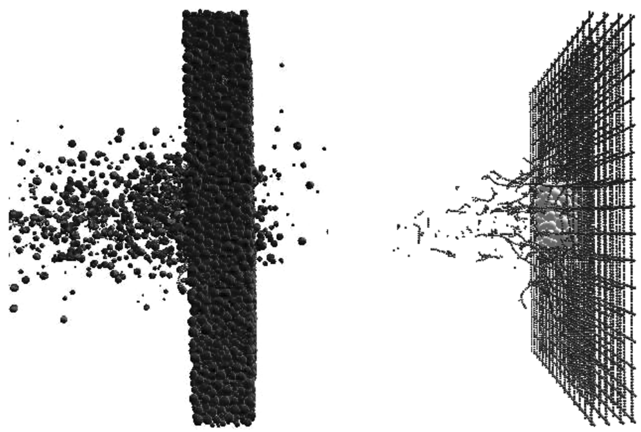

Fig. 8 Snap shot of impact reference test at t = 11 ms with impact velocity = 151 m/s

implemented. The different results are shown in Fig. 9, where the target and the position of the rebars are given on the vertical axis.

Both, the elastic-brittle law obtained with PFC^{3D} and the elastic-plastic-damage law obtained with YADE predict the penetration depth of the missile in the slab, as a function of time. If focusing on the compaction process during the first milliseconds after impact, as displayed in the YADE code, the amount of interaction forces in the concrete slab reaching the hardening stage remains low with only 1.5% while 50% of the interactions are under tension loading (Fig. 10).

Thus, for the reference case, most of the compaction involves a densification of the arrangement of the spherical discrete elements close to the impactor, whereas the amount of interaction forces reaching the hardening zone (which corresponds to higher stage of compaction) remains low. This kind of response for an impacted concrete wall, where a low compaction process occurs, is possible when:

1. the impact velocity is low, which produces an elastic wave propagation,
2. the missile's nose is flat, which increases the amplitude of this elastic wave,
3. the thickness of the target (0.208 m) is on the same order as the missile's diameter (0.278 m), which amplifies the scabbing process.

As soon as the scabbing process takes place, the back fracturing zone reaches the one located next

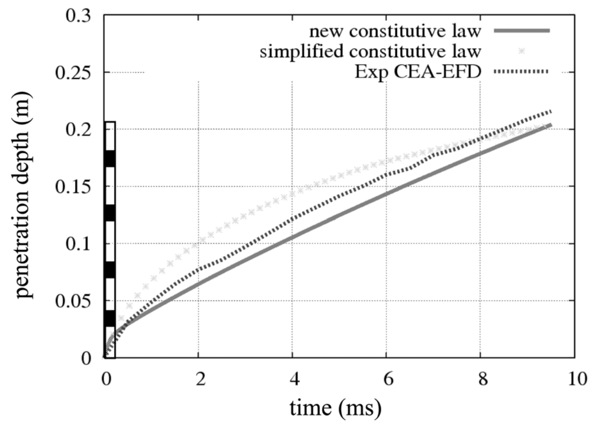

Fig. 9 Comparison of the trajectory of the missile with different local constitutive laws. Solid, dotted and starred lines are, respectively, experiments, elastic-bilinear hardening-damage constitutive law and elastic-brittle constitutive law. The thickness of the target is given on the y-axis with a dark rectangular bar, where the black dots correspond to the rebars' positions

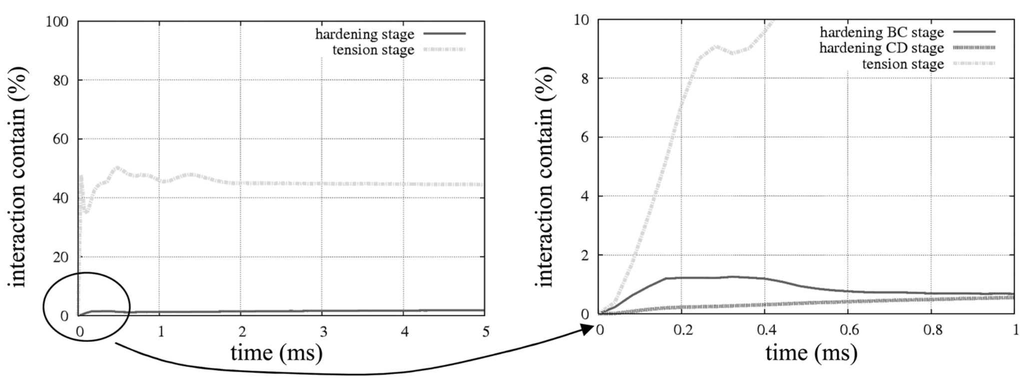

Fig. 10 On the left, the evolution of the amount of interaction forces which have reached the hardening stage and the tension stage in the concrete slab. On the right, the detailed diagram of the first ms

to the missile creating a cone plug, which facilitates the missile progression (Shiu, *et al*. 2008b, Magnier and Donzé 1998).

Thus, in this case, a basic local elastic-brittle constitutive law is sufficient to predict the penetration or the perforation of a missile in a thin concrete target at low impact velocities, with, however, a slightly better prediction for the more complete constitutive law.

3.3. Compaction process due to the impact velocity and the missile diameter

While keeping the same configuration test, the impact velocity is now increased from 151 m/s to 500 m/s. The new trajectory of the missile is presented in Fig. 11: the missile has now completely perforated the target.

In Fig. 12, the extension of the compacted zone inducing the hardening process at the local scale for the two different impact velocities at t = 0.5 ms are shown. A dramatic increase of the compacted zone is observed when the impact velocity increases.

For higher impact velocities, it is observed that the back fracturing zone doesn't have enough time

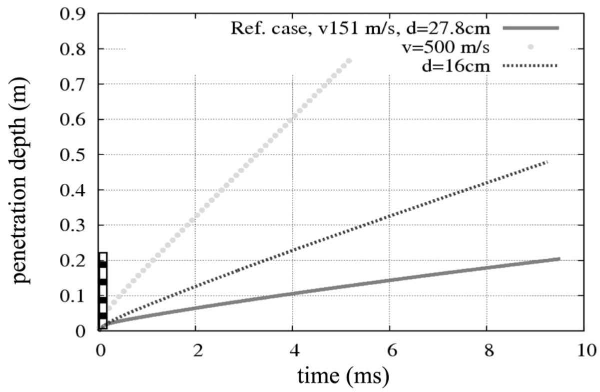

Fig. 11 Comparison of the trajectory of the missile for different impact cases. The lower, middle and upper lines are, respectively, the reference case, the case using a 16 cm wide missile with the same initial kinetic energy and the case with an impact velocity of 500 m/s. The thickness of the target is given on the y-axis with a dark rectangular bar, where the black dots correspond to the rebars' positions

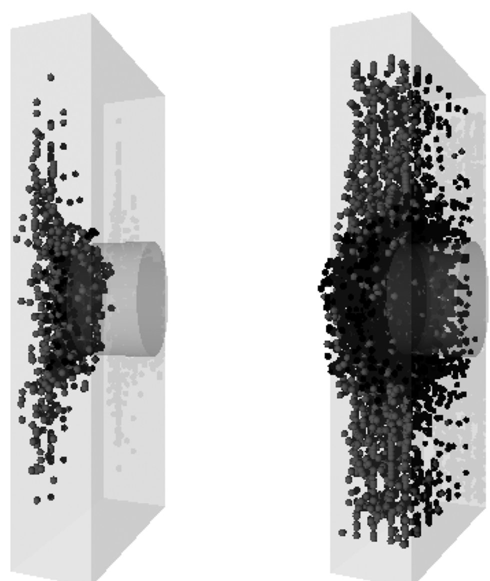

Fig. 12 Snapshots of local interaction forces in the hardening stage, at t = 0.35 ms of missile impact with v = 151 m/s, which is the reference case (left) and v = 500 m/s (right)

to reach the area located next to the missile. This induces a constant compaction process in front of the impactor and indeed, the interaction force recording data, indicates that the hardening zone has reached 7% of the interaction forces instead of the former 1.5%.

Another simulation was made by decreasing the missile diameter to 0.16 m, instead of 0.278 m, while keeping the same kinetic energy as in the reference case. To do so, the impact velocity was kept constant at 151 m/s, whereas the density was increased.

In this case, where the ratio between the thickness of the target and the diameter of the missile has increased, it was observed that the missile could perforate the target more easily than in the

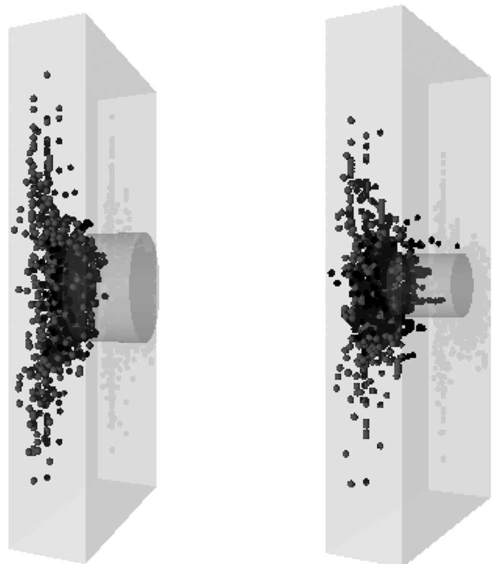

Fig. 13 Snap shots of local interaction forces in the hardening stage, at t = 0.5 ms of missile impact with v = 151 m/s , which is the reference case (left) and a missile with a diameter of 16 cm with the same initial kinetic energy (right)

reference case (see Fig. 10) and no scabbing process occurred. Thus, the compressive elastic wave generated by this smaller impactor did not have enough energy to create tensile fractures on the back side of the target. More of the kinetic energy is spent on the local compaction process during penetration and less dissipates in wave propagation. Even though, the amount of interaction forces in the concrete slab reaching the hardening stage is comparable to the reference case (about 1.41%), the highly compacted zone remains located close to the missile (Fig. 13).

3.3. Numerical model compared to penetration and perforation prediction laws

It has been shown that using both, an elastic-brittle constitutive law and an elastic-bilinear hardening-damage constitutive law, correctly predicts the trajectory of the missile perforating a concrete slab as a function of time for which its thickness is about the missile diameter size. Keeping the missile diameter constant, let us see how these two behavior laws act on the penetration and/or perforation of the missile. To investigate this new configuration, the results of the simulations are compared to two validated prediction laws which are the Li and Chen formula (Li and Chen 2003) for the penetration and the Fullard, *et al*. formula (1991) for the perforation (the formulation of these prediction laws are given in appendix A). For this purpose, a simulation with a concrete slab of 0.8 m thickness and a missile diameter of 0.2 m has been set up. For an impact velocity of 90 m/s, the mass of the missile was varied from 50 kg up to 600 kg. Since the predictions laws cited earlier take into account the mass of the missile, it will be used for this parametric study.

On Fig. 14, the shaded area on the right indicates the domain for which the missile is supposed to perforate the concrete slab, according to Fullars's prediction law (which is an upgrade of Berriaud's prediction law, since it takes into account the amount of reinforcement). The dash-point curve corresponds to Li and Chen's formula (which is named “empirical prediction” on the Figure), and it

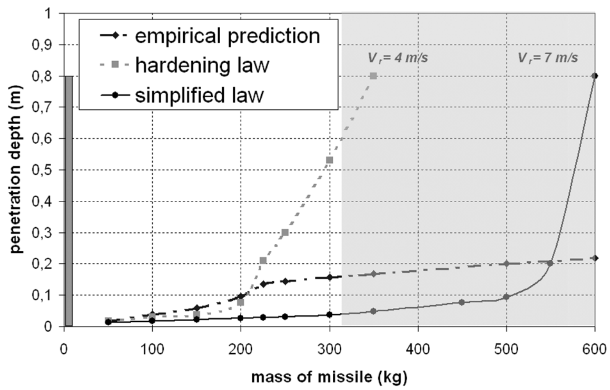

Fig. 14 Penetration depth v.s. the mass of the missile. The thickness of the target is given on the y-axis with a dark rectangular bar. The shaded area on the right indicates that the concrete slab is perforated according to Fullar's prediction law. The dashed-point curve corresponds to Li & Chen's prediction law for penetration, the plain curve corresponds to the local simplified elastic constitutive law and the dotted curve corresponds to the local elastic-bilinear hardening-damage constitutive law

corresponds to the maximum penetration of the missile in a semi-infinite medium.

When using a discrete element model with an elastic-brittle constitutive local law, the evolution of the missile penetration is given by the black plain curve (Fig. 14). It can be observed that, when the mass is low, the penetration depth is lower than the one predicted by Li and Chen's formula. Moreover, the missile perforates the concrete slab when its mass is just below 600 kg (at 600 kg, the residual velocity of the missile on the back side of the target is about 7 m/s), whereas Fullard's law predicted a perforation for a mass of 310 kg. Thus, the use of this elastic-brittle constitutive local law in the Discrete Element Model induces such a large difference with the two prediction laws, that it can not be acceptable to predict the penetration and perforation of large concrete targets.

Increasing the thickness of the target gives a more significant ratio between the thickness and the diameter of the missile. Thus, the impact penetration process must go through a hardening stage.

Now, when using the elastic-bilinear hardening-damage constitutive law in the numerical model (see Fig. 14), it has been observed that for small masses, the maximum penetrations obtained for the missile are close to the ones predicted by Li and Chen's formula and the perforation of the target is also obtained for a mass which was predicted by Fullard's prediction law. Thus, the use of the local hardening constitutive law gives results in penetration and perforation which are closer to empirically predicted results than those of a local elastic constitutive law. It is interesting to note that the model is also capable of giving new insights into the penetration process when the reflecting waves create the scab and the cone plug is deep enough to join the maximum penetration depth (Li, *et al.* 2005, Shiu, *et al.* 2008b): this induces a sudden dramatic increase of the penetration in the domain of the "just perforation" configuration (here obtained for a mass around 200-250 kg as shown in Fig. 14).

4. Conclusions

A local elastic-bilinear hardening-damage constitutive law is developed to study the behavior of a concrete slab under extreme dynamic loading. The numerical model was constructed based on a 3D discrete element approach. The local parameters have been calibrated with a set of static tests where a simple compression test and a hydrostatic test (650 MPa) were simulated. The static simulation results agreed well with the experimental data. After finishing the calibration process, the simulation of a full reinforced concrete target impacted by a rigid missile was performed. The first results show that for a thin target, both the brittle-elastic law and the elastic-bilinear hardening-damage constitutive law can well predict the penetration depth caused by the missile. In fact in the reference case, even if compaction can be seen it is nonetheless a minor part of the impact process while tensile fracturing is the major component. Thus a brittle-elastic law is sufficient to predict the response of the target in this case.

However, in order to go beyond this reference case two additional tests were then simulated. In the first one, the impact velocity was raised from 151 m/s to 500 m/s resulting in dramatically increased compacted zone, as expected. In the second one, to reduce the effect of scabbing, the ratio between the thickness of the target and the diameter of the missile was increased while keeping the kinetic energy constant. This was done by decreasing the diameter of the missile and increasing its density. This resulted in the same amount of compaction as in the reference case but differently distributed. Close to the missile head, compaction was more intense. In addition, the missile completely perforated the slab which it hadn't done in the reference case. To evaluate the contribution of the compaction process using the hardening law in a quantitative manner, impact simulations on a thicker target (i.e. with a thickness larger than the missile diameter) have been compared to widely used prediction laws for penetration and perforation. It turned out that since the model uses a local hardening interaction force formulation, it was capable of reproducing the maximum penetration and predict the perforation limit in a better way than just using a local elastic law.

References

Belheine, N., Plassiard, J.-P., Donzé, F.-V., Darve, F. and Seridi, A. (2008), "Numerical simulation of drained triaxial test using 3d discrete element modeling", *Comput. Geotech.*, DOI 10.1016/j.compgeo. 2008.02.003.

Berriaud, C., Sokolovsky, A., Gueraud, R., Dulac, J. and Labrot, R. (1978), "Local behavior of reinforced concrete walls under missile impact", *Nucl. Eng. Des.*, **45**(2), 457-469.

Burlion, N. Gatuingt, F., Pijaudier-Cabot, G. and Daudeville, L. (2000), "Compaction and tensile damage in concrete: constitutive modelling and application to dynamics", *Comput. Methods Appl. Mech. Eng.*, **183**(3-4), 291-308.

Cundall, P. A. and Strack, O. D. L. (1979), "A discrete numerical model for granular assemblies", *Géotechnique*, **29**(1), 47-65.

Donzé, F. V., Magnier, S.-A., Daudeville, L., Mariotti C. and Davenne, L. (1999), "Study of the behavior of concrete at high strain rate compressions by a discrete element method", *ASCE J. Eng. Mech.* **125**(10), 1154-1163.

Fullard, K., Baum, M. R. and Barr, P. (1991), "The assessment of impact on nuclear power plant structures in the United Kingdom", *Nucl. Eng. Des*., **130**(113-20).

Gabet, T., Malecot, Y. and Daudeville, L. (2008). "Triaxial behaviour of concrete under high stresses: influence of the loading path on compaction and limit states", *Cement Concrete Res.*, **38**(3), 403-412.

Hentz, S., Donzé, F. V. and Daudeville, L. (2004a), "Discrete element modelling of concrete submitted to dynamic loading at high strain rates", *Comput. Struct.*, **82**(29-30), 2509-2524.

Hentz, S., Daudeville, L. and Donzé, F. V. (2004b), "Identification and validation of a discrete element model for concrete", *J. Eng. Mech*., **130**(6), 709-719.

Iwashita, K. and M., Oda, M. (2000), "Micro-deformation mechanism of shear banding process based on modified distinct element method", *Powder Technology.* **109**, 192205.

Kozicki, J. and Donzé, F. V. (2007), "Applying an open-source software for numerical simulation using finite element or discrete modeling methods", *Comput. Methods Appl. Mech. Eng.*, submitted, to appear.

Li, Q. M. and Chen, X. W. (2003), "Dimensionless formulae for penetration depth of concrete target impacted by

a non-deformable projectile", *Int. J. Impact. Eng.* **28**(1), 93-116.
Li, Q. M., Reid, S. R., Wen, H. M. and Telford, A. R. (2005), "Local impact effects of hard missiles on concrete targets", *Int. J. Impact. Eng.* **32**(1-4), 224-284.
Magnier, S. A. and Donzé, F. V. (1998), "Numerical simulation of impacts using a discrete element method", *Mech. Cohes.-frict. Mater.* **3**, 257-276.
PFC^{3D} (Particle Flow Code in 3 Dimensions), Version 3.0. (2003), *Itasca Consulting Group Inc.*, Minneapolis, Minnesota.
Shiu W., Donzé F.-V. and Daudeville. L. (2008a), "Discrete element modelling of missile impacts on a reinforced concrete target", *Int. J. Computer Appl. Tech. submitted.*
Shiu, W., Donzé F.-V. and Daudeville L. (2008b), "Penetration prediction of missiles with different nose shapes by the discrete element approach", *Comput. Struct.*, doi: 10.1016/j.comp struc.2008.03.003.
YADE, Open Source Discrete Element Code (2004), http://yade.wikia.com/wiki/Yade

Appendix A

The prediction of the penetration depth formulated by Li and Chen (2003), is given by:

$$\frac{x}{d} = \sqrt{\frac{(1+(k\pi/4N))}{(1+(I/N))}\frac{4k}{\pi}I} \quad \text{for } \frac{x}{d} \le k \tag{9}$$

$$\frac{x}{d} = \frac{2}{\pi}N ln\left[\frac{1+(I/N)}{1+(k\pi/4N)}\right]+k \quad \text{for } \frac{x}{d} > k \tag{10}$$

where I and N are the impact function and the geometry function respectively which can be expressed by:

$$I = \frac{1}{72f_c^{-0.5}}\frac{MV_0^2}{d^3 f_c} \tag{11}$$

$$N = \frac{1}{N^*}\frac{M}{\rho_c d^3} \tag{12}$$

where f_c is the unconfined compressive strength of concrete, ρ_c is the density of concrete, M, V_0 and d are respectively the mass, the impact velocity and the diameter of the missile. N^* is the nose shape factor. For a flat nose missile, the value of the N^* is equal to 1. Finally, $k = \left(0.707+\frac{h}{d}\right)$, where h is the length of the projectile nose.

In the case of a shallow penetration, if $x/d < 5.0$, the penetration depth is given by:

$$\frac{x}{d} = 1.628\left(\frac{1+(k\pi/4N)}{1+(I/N)}\frac{4k}{\pi}I\right)^{1.395} \tag{13}$$

The prediction of the perforation can be expressed by the ballistic limit velocity (V_p), which can be evaluated by the formula proposed by Fullard (Fullard, *et al*. 1991):

$$V_p = 1.3\rho_c^{1/6}f_c^{0.5}\left(\frac{dH_o^2}{M}\right)^{2/3}(r+0.3)^{0.5} \tag{14}$$

where H_0 is the thickness of the target and r is the reinforcement ratio described by the percentage "*each way in each face*" (*% EWEF*). The reinforcement ratio is equal to 0 for the present case of study.